

Wdr5 Mediates Self-Renewal and Reprogramming via the Embryonic Stem Cell Core Transcriptional Network

Yen-Sin Ang,^{1,2,3,*} Su-Yi Tsai,^{1,3,5} Dung-Fang Lee,^{1,2,3,7} Jonathan Monk,^{1,2,7} Jie Su,^{1,2,3,7} Kajan Ratnakumar,^{1,4,5} Junjun Ding,^{1,3} Yongchao Ge,⁶ Henia Darr,^{1,2,3} Betty Chang,^{1,2,3} Jianlong Wang,^{1,3} Michael Rendl,^{1,3,5} Emily Bernstein,^{1,4,5,7} Christoph Schaniel,^{1,2,7} and Ihor R. Lemischka^{1,2,3,*}

¹Black Family Stem Cell Institute

²Department of Gene and Cell Medicine

³Department of Developmental and Regenerative Biology

⁴Department of Oncological Sciences

⁵Department of Dermatology

⁶Department of Neurology

Mount Sinai School of Medicine, New York, NY 10029, USA

⁷These authors contributed equally to this work

*Correspondence: yen-sin.ang@mssm.edu (Y.-S.A.), ihor.lemischka@mssm.edu (I.R.L.)

DOI 10.1016/j.cell.2011.03.003

SUMMARY

The embryonic stem (ES) cell transcriptional and chromatin-modifying networks are critical for self-renewal maintenance. However, it remains unclear whether these networks functionally interact and, if so, what factors mediate such interactions. Here, we show that WD repeat domain 5 (Wdr5), a core member of the mammalian Trithorax (*trxG*) complex, positively correlates with the undifferentiated state and is a regulator of ES cell self-renewal. We demonstrate that Wdr5, an “effector” of H3K4 methylation, interacts with the pluripotency transcription factor Oct4. Genome-wide protein localization and transcriptome analyses demonstrate overlapping gene regulatory functions between Oct4 and Wdr5. The Oct4-Sox2-Nanog circuitry and *trxG* cooperate in activating transcription of key self-renewal regulators, and furthermore, Wdr5 expression is required for the efficient formation of induced pluripotent stem (iPS) cells. We propose an integrated model of transcriptional and epigenetic control, mediated by select *trxG* members, for the maintenance of ES cell self-renewal and somatic cell reprogramming.

INTRODUCTION

The maintenance of ES cell self-renewal requires a network of transcription factors, including Oct4, Sox2, Nanog, Esrrb, Tbx3, and Tcf3 (Chen et al., 2008; Ivanova et al., 2006; Kim et al., 2008; Tam et al., 2008). These factors participate in auto- and cross-regulatory interactions to increase their own expression and that of other self-renewal-associated genes while repressing

genes that promote differentiation. Perturbation of these factors collapses the self-renewal circuitry and triggers specific or mixed lineage differentiation (Ivanova et al., 2006). In contrast to the numerous transcription factors, only a handful of chromatin regulators that are important for self-renewal have been characterized (Loh et al., 2007; Pasini et al., 2007; Schaniel et al., 2009).

ES cells harbor an open, transcriptionally permissive chromatin that allows for efficient epigenomic remodeling during lineage commitment (Efroni et al., 2008). However, factors regulating this “hyperdynamic” epigenetic configuration remain poorly understood. ES cells also contain “bivalent domains” where nucleosomes are marked by trimethylation at histone3-lysine27 (H3K27me3) and histone3-lysine4 (H3K4me3) (Bernstein et al., 2006). The Polycomb group (*PcG*) complex mediates H3K27me3, correlated with gene repression (Boyer et al., 2006). In contrast, the Trithorax group (*trxG*) complex mediates H3K4me3, generally correlated with gene activation (Ringrose and Paro, 2004). Although *PcG* has been extensively investigated in the maintenance of ES cell self-renewal, pluripotency, and somatic cell reprogramming, there exists little complementary information for *trxG*-associated members. This imbalance of knowledge represents a significant shortcoming in the understanding of the roles played by trimethylated H3K4 and H3K27 in regulating the ES cell identity. Moreover, it remains to be shown whether the well-established transcriptional network can functionally interact with epigenetic regulators to maintain pluripotency and, more importantly, which factors mediate such interactions.

An unresolved question in chromatin biology is the manner by which generic histone modification complexes, like *PcG* and *trxG*, become targeted to specific genomic loci to direct specific gene regulatory functions (Schuettengruber et al., 2007). This is especially intriguing in the context of ES cells. For example, Chd1, a chromodomain-helicase-DNA-binding protein that is not specific to ES cells, was recently described to be essential for pluripotency and reprogramming (Gaspar-Maia et al.,

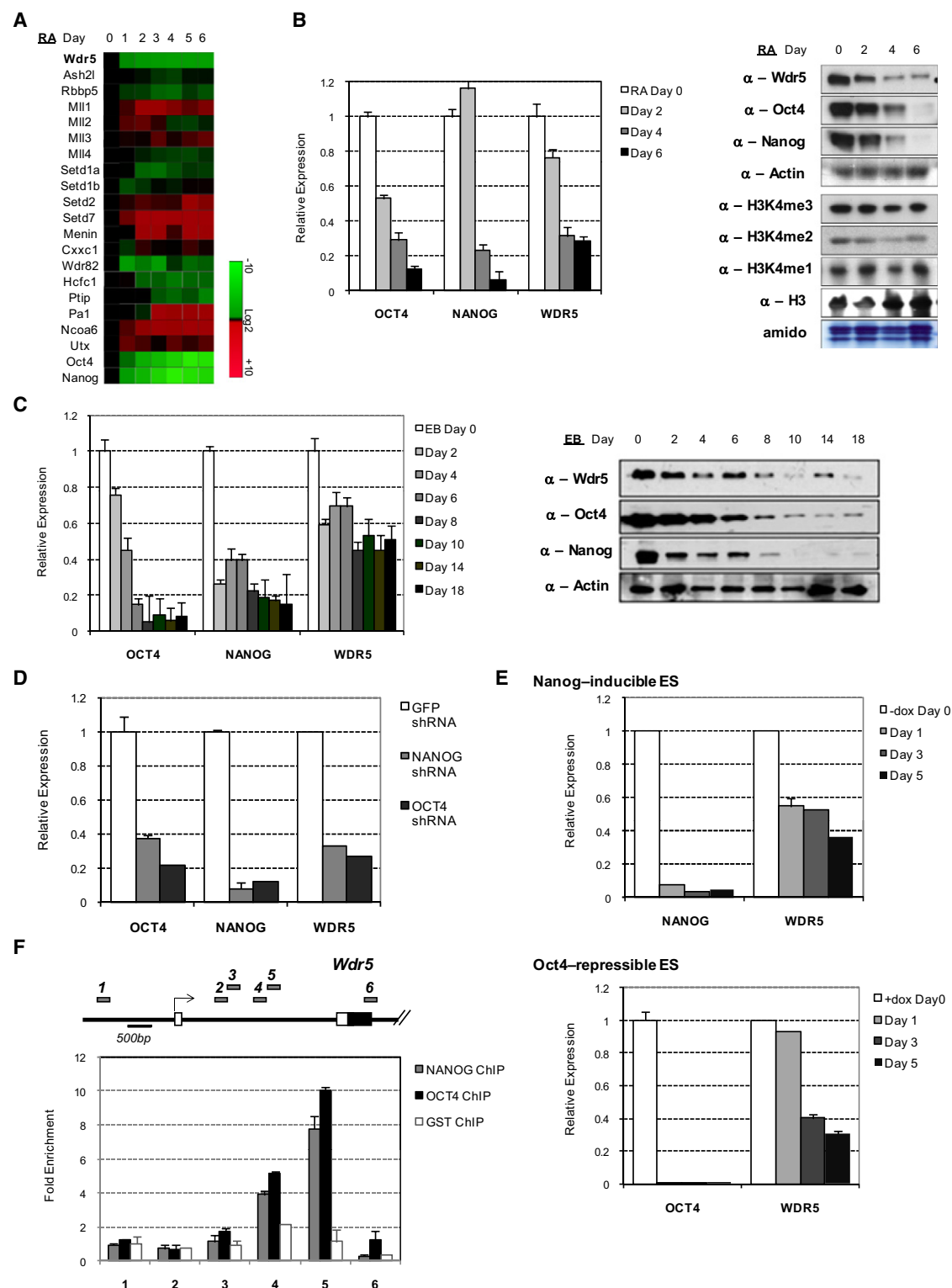


Figure 1. Downregulation of Wdr5 Expression upon ES Cell Differentiation

(A) Heatmap of *trxG*-associated member expressions during RA induction from Ivanova et al. (2006).

(B and C) Real-time PCR (left) and immunoblot (right) analyses during RA induction and EB formation.

(D) Real-time PCR analysis after 3 days shRNA knockdown of Nanog and Oct4.

2009). The factor(s) or mechanism(s) conferring such functional specificity to epigenetic regulators remains unknown. Moreover, it is unclear how ectopic expression of four transcription factors—Oct4, Sox2, Klf4, and c-Myc (OSKM)—can reprogram somatic cells to iPS cells with epigenomes that are largely indistinguishable from ES cells (Carvajal-Vergara et al., 2010; Tsai et al., 2010). This is especially pertinent to the re-establishment of the bivalent signature. Interestingly, although the OSKM-iPS methodology has been replaced by various combinations of factors or small molecules, Oct4 remains the sole factor that, until recently, could not be substituted/omitted (Heng et al., 2010). Accordingly, we reasoned that the resetting of the somatic epigenome must be achieved through the activity of Oct4-interacting proteins and/or Oct4 target genes.

Protein complexes of the Set/MLL histone methyltransferase (HMT) family are mammalian homologs of *trxG* that function as conserved, multisubunit ensembles to catalyze the methylation of H3K4. The human *MLL* gene, which contains a SET domain, was first identified based on translocations that are commonly associated with the pathogenesis of multiple forms of hematological malignancies (Shilatifard, 2006). Notably, Set/MLL proteins alone are catalytically inactive but require core subunits—Wdr5, Ash2l and Rbbp5—that are related to components of the yeast Set1 complex (Dou et al., 2006). The Rbbp5 and Ash2l heterodimer directly participates in HMT activity of the MLL1 complex (Cao et al., 2010). Ash2l is required for mouse embryogenesis (Taylor et al., 2010) and proper X-inactivation (Pullirsch et al., 2010), whereas diminished recruitment of Rbbp5 is found in patients with Wiskott-Aldrich syndrome (Stoller et al., 2010). Other *trxG*-associated cofactors such as Menin, Hcf1, and Cxxc1 have been implicated in processes like pancreatic β cell growth (Karnik et al., 2007), tumorigenesis (Lairmore and Chen, 2009), apoptosis (Tyagi and Herr, 2009), and euchromatin formation (Thomson et al., 2010). In particular, Wdr5 is a key component of *trxG* acting as a “presenter” of the H3K4 residue and is indispensable for Set/MLL complex assembly and effective HMT activity (Dou et al., 2006). It was shown that Wdr5 interacts with H3K4me2 and mediates transition to the trimethylated state (Wysocka et al., 2005). However, it was also shown that Wdr5 is unable to distinguish between different H3K4 methylation states (Couture et al., 2006). Although Wdr5 function is required for vertebrate development (Wysocka et al., 2005) and osteoblast differentiation (Zhu et al., 2008), its role in ES or iPS cells remains to be determined.

RESULTS

Wdr5 Expression Positively Correlates with the Undifferentiated ES Cell State

We sought to functionally characterize specific chromatin regulators in the maintenance of ES cell self-renewal, with a particular focus on *trxG*-associated members. For this, we

mined our previous microarray data (Ivanova et al., 2006) and published iPS cell data sets for expressions of *trxG* complex members. Wdr5 emerged as an obvious candidate, as its expression was downregulated upon differentiation (Figure 1A) and upregulated during iPS cell formation (Figure S1A), unlike other members whose expression levels were incoherent among the data sets. Interestingly, the upregulation of Wdr5 in iPS cells was independent of the somatic cell types chosen for reprogramming. We also observed higher Wdr5 and H3K4me3 levels in ES cells than in somatic cells and tissues (Figures S1B and S1C), suggesting specific Wdr5 functions in ES and iPS cell maintenance.

We next validated our microarray data and observed a marked Wdr5 reduction, similar to Oct4 and Nanog, with concomitant decreases in global H3K4me3 (Figure 1B). Wdr5 diminution in embryoid body (EB) assays indicated that this was not specific to retinoid acid (RA) induction but was generally representative of differentiation (Figure 1C). Additionally, when we depleted Oct4 or Nanog using short hairpin RNA (shRNA), we also observed a reduction in Wdr5 (Figure 1D). This effect was not unique to the shRNAs, as Wdr5 decreases were also observed using the Nanog-inducible and Oct4-repressible ES cell lines (Figure 1E). Furthermore, chromatin immunoprecipitation (ChIP) confirmed Oct4 and Nanog occupancy in intron 1 of *Wdr5* (Figure 1F). These data indicate that Wdr5 expression correlates positively with the undifferentiated state and that the *Wdr5* gene is a downstream target of Oct4 and Nanog.

Wdr5 Is a Regulator of ES Cell Self-Renewal

We next designed shRNAs targeting Wdr5 to determine whether it is required for self-renewal. Wdr5 shRNA-2 and -4 effectively depleted Wdr5 mRNA and protein levels, but not those encoding other WD repeat proteins (Figure 2A and Figure S1D). Wdr5 knockdown induced changes in cell morphology and decreased alkaline phosphatase (AP) activity, indicative of differentiation (Figure 2B). In ES cell competition assays, Wdr5 depletion resulted in loss of self-renewal similar to depletion of LIF receptor (LIFR) or Nanog (Figure 2C). Furthermore, depletion of Wdr5 diminished secondary ES colony formation (Figure 2D) and reduced self-renewal gene expression while increasing ectodermal and trophectodermal gene expressions (Figure S1E). Importantly, Wdr5 depletion induced the collapse of the extended ES cell transcriptional network (Figure 2E).

To rule out shRNA off-target effects, we built complementation “rescue” ES cell lines (Wdr5R) where endogenous Wdr5 was constitutively repressed by Wdr5-shRNA and rescued by a Doxycycline-inducible (Dox) shRNA-immune Wdr5 (Figure 2F). Removal of Dox resulted in loss of self-renewal gene expression in two independent clones, whereas, in the presence of Dox, expression remained at normal levels (Figure 2F, right). This was also evident from AP staining (Figure S2A). Global gene expression profiling and gene set enrichment analyses (GSEA)

(E) Real-time PCR analysis in Nanog-inducible (Ivanova et al., 2006), Oct4-repressible lines (Schanuel et al., 2009). All data are normalized to actin and shown relative to day 0 or GFP shRNA.

(F) ChIP-qPCR analysis of Oct4 and Nanog occupancy at *Wdr5* locus. Numbered gray bars indicate primer locations. Glutathione S transferase (GST) ChIP as negative control. Values are expressed as fold enrichment relative to input DNA and a control region (Loh et al., 2007).

Data are represented as mean \pm SD; n = 3. See also Figure S1.

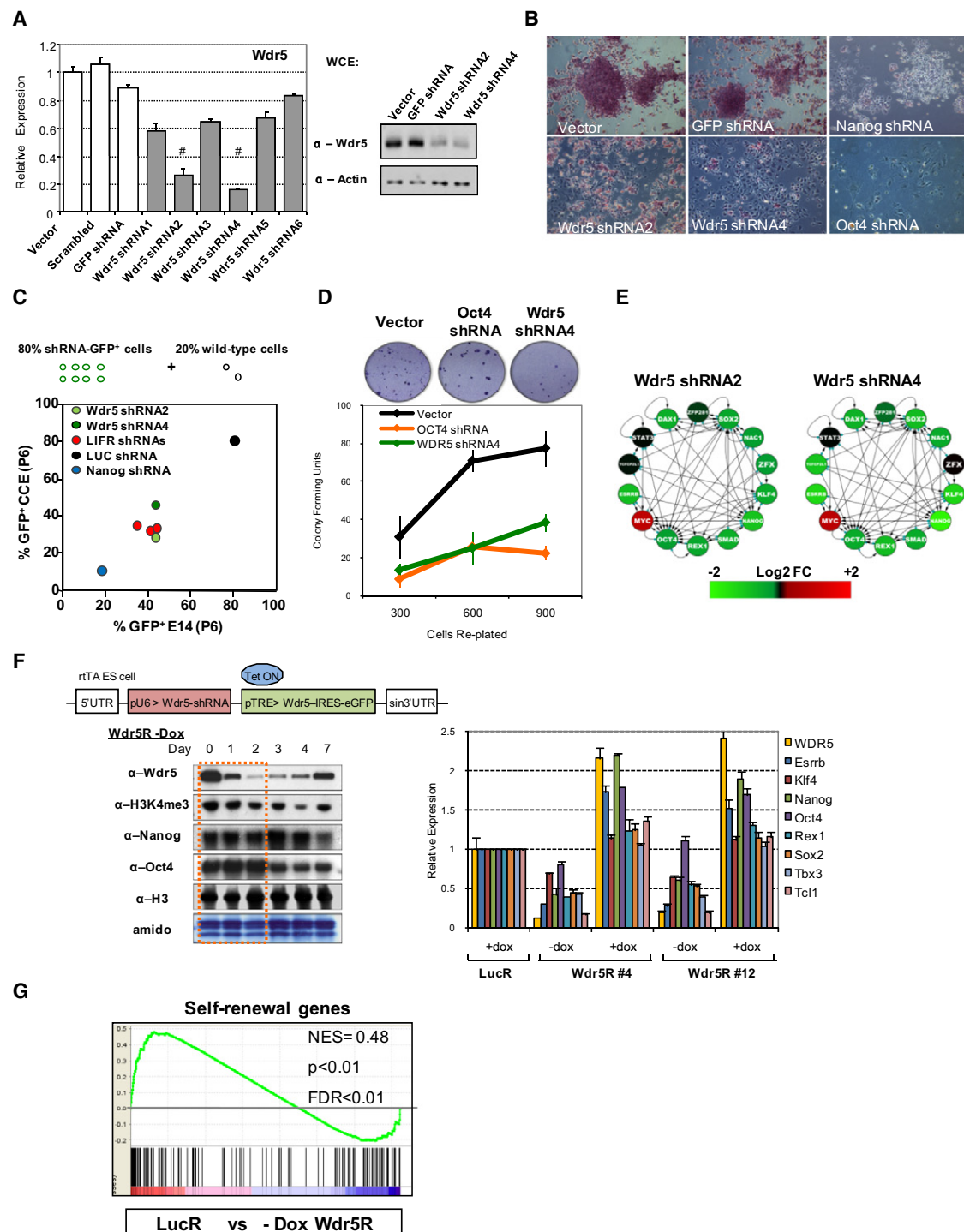


Figure 2. Wdr5 Depletion Results in Loss of Self-Renewal and Collapse of Extended Transcriptional Network

(A) Real-time PCR (left) and immunoblot (right) analyses after 4 days Wdr5 knockdown.

(B) AP staining after 4 days shRNA knockdown.

(C) ES cell competition assay (Ivanova et al., 2006) in E14 and CCE cells. Luciferase (LUC), Nanog, and LIFR shRNAs serve as negative and positive controls, respectively.

(D) Secondary ES colony replating assay (Tay et al., 2008). Circles depict colonies from the 600 cell-replated wells.

(E) Gene expression of composite transcriptional network (Chen et al., 2008; Kim et al., 2008) after 4 days Wdr5 depletion as measured by real-time PCR. Log₂ fold change relative to GFP shRNA.

demonstrated that Wdr5 depletion repressed self-renewal and enhanced primarily ectoderm differentiation (Figure 2G and Figure S2B). Gene ontology (GO) analysis of the differentially expressed genes revealed enrichment in categories like developmental processes, mesoderm and skeletal development, and others (Figure S2C). Arguing against induced apoptosis or a general loss of proliferative potential, Wdr5 depletion in ES cells resulted in no change in apoptotic gene expressions, whereas cell-cycle analysis showed only a marginal impediment (Figures S2D and S2E). Indeed, sporadic clusters of viable cells expressing lineage-specific markers, nestin and smooth muscle actin, were detectable after extended periods of Wdr5 knockdown (Figure S2F). In addition, Wdr5 depletion in fibroblasts and myoblasts induced no significant changes in cell cycle, suggesting that Wdr5 has specific roles in maintenance of ES cell self-renewal (Figure S2G–S2I).

We next asked whether Wdr5 overexpression was sufficient to block differentiation in EB assays using the Wdr5R (Figure S2J). Wdr5 overexpression (+Dox) delayed trophectoderm and mesoderm differentiation (Figures S2K and S2L) and enhanced endoderm differentiation (Figure S2N) but failed to prevent loss of self-renewal genes (Figure S2O). Conversely, Wdr5 repression enhanced commitment to trophectoderm and endoderm yet accelerated the loss of self-renewal markers (Figures S2K, S2N, and S2O). The enhanced differentiation following knockdown of Wdr5 also argues against a general loss of cell viability. Finally, transient overexpression of Wdr5 under self-renewing conditions resulted in no change in ES cell identity (data not shown). Collectively, these results show that Wdr5 plays specific roles in maintaining an intact ES cell transcriptional network and, consequently, a self-renewal phenotype but is insufficient to block differentiation.

Wdr5 Maintains Global and Localized H3K4 Trimethylation

We further pursued the mechanism by which Wdr5 regulates self-renewal. Wdr5 is known to be required for H3K4me3 modification and HOX gene activation (Wysocka et al., 2005). As expected, Wdr5 knockdown reduced the amount of Wdr5 in chromatin and global H3K4me3 levels (Figure 3A). Moreover, we observed that the reduction in H3K4me3 precedes downregulation of Oct4, Nanog, or SSEA1 markers (Figure 2F, left). At 2 days after Wdr5 depletion, whereas no change in Oct4 or Nanog levels was detectable, H3K4me3 levels were evidently reduced by more than 50%. This diminution continued and became more marked at day 4. We reason that H3K4me3 reduction is even more significant at day 4, after the initiation of Oct4 downregulation, because *Wdr5* is a downstream target gene of Oct4. Thus, depletion of Oct4 could further attenuate the transcription of Wdr5 and, consequently, expression levels of global H3K4me3. Additionally, a significant SSEA1 decrease was only

detected after day 3 (Figure S3A). These data indicate that loss of H3K4me3 is a direct result of Wdr5 depletion and not an indirect result of the loss of pluripotency factors such as Oct4 or Nanog.

We further detected decreases in H3K4me3 at the *Pou5f1* and *Nanog* loci upon Wdr5 depletion (Figure 3B). H3K4me3 reduction also occurred at pluripotency-associated gene promoters where we had shown decreased expression levels (Figure 3C), as well as at “bivalent” promoters and at other promoters (Figure S3B). In line with the role of H3K4me3 in RNA polymerase II (RNAP-II) recruitment (Wang et al., 2009), Wdr5 loss reduced RNAP-II occupancy at *Nanog*, *Sox2*, *Fbx15*, and *Myc* genes (Figure 3D). Moreover, using a Nanog-reporter line (Schaniel et al., 2009), Wdr5 depletion reduced Nanog promoter activity (Figure S3C). Knockdowns of two other *trxG*-associated members Ash2l and Menin (Shilatifard, 2006) also induced ES cell differentiation (Figure S3D). This strongly suggested that the maintenance of self-renewal requires elevated H3K4me3 expression. Collectively, these data indicate that Wdr5 is critical for the maintenance of global and localized H3K4me3 and for transcriptional activation in ES cells.

Wdr5 Interacts with Oct4 in ES Cells

The indispensable role of Wdr5 in self-renewal suggested probable physical interactions with components of the core transcriptional network. Coimmunoprecipitation (co-IP) using an Oct4 antibody demonstrated an interaction with Wdr5 (Figure 4A). To confirm the Wdr5-Oct4 interaction, we derived ES cell lines in which Wdr5 was tagged with Flag or Myc epitopes and selected for clones that had minimum Wdr5 overexpression (Figure S4A). Additionally, we measured self-renewal and differentiation markers to pick clones that were statistically indistinguishable from the control line (Figures S4B and S4C). A resultant Wdr5_{FL2} line had typical growth rates and morphology and was capable of in vitro and in vivo differentiation (Figures S4D–S4F), demonstrating bona fide pluripotency. Using this line, we successfully co-IPed Wdr5 with Oct4 (Figure 4A), as well as Nanog and Sox2 (data not shown). Co-IP of other *trxG*-associated members, Rbbp5 and Menin, suggested that these factors exist in functionally active protein complexes. We next performed a gel filtration experiment to ask whether Oct4 is part of the larger *trxG* complex (Figure 4B). We observed that, whereas Oct4 is enriched primarily at molecular weight (MW) fractions between 150 and 50 kDa and Wdr5, Ash2l, and Rbbp5 are enriched primarily at > 600 kDa MW fractions, there were several fractions in which substantial amounts of Oct4 coeluted with the core *trxG*-associated proteins (Figure 4B, orange box). Interestingly, we also observed Wdr5 to be the major protein coeluting at peak Oct4 fractions in the absence of Ash2l or Rbbp5 (Figure 4B, blue). This suggests that the Wdr5-Oct4 partnership might extend beyond HMT activity alone.

(F) Scheme of tetracycline-inducible Wdr5 rescue construct (top). Immunoblot analysis after Dox withdrawal in Wdr5R #4 (left). Orange box shows H3K4me3 reduction preceding the loss of Oct4 and Nanog. Real-time PCR analysis (right) after 5 days Wdr5 knockdown (–dox) or with rescue (+dox) in two clones (Wdr5R #4 and #12). All data are normalized to actin and shown relative to Vector, GFP shRNA, or Luc rescue clone (LucR). Data are represented as mean ± SD; n = 3. (G) GSEA of a gene set representing self-renewal markers upon Wdr5 knockdown. NES, normalized enrichment score; p = nominal p value; FDR = false discovery rate.

See also Figure S1 and Figure S2.

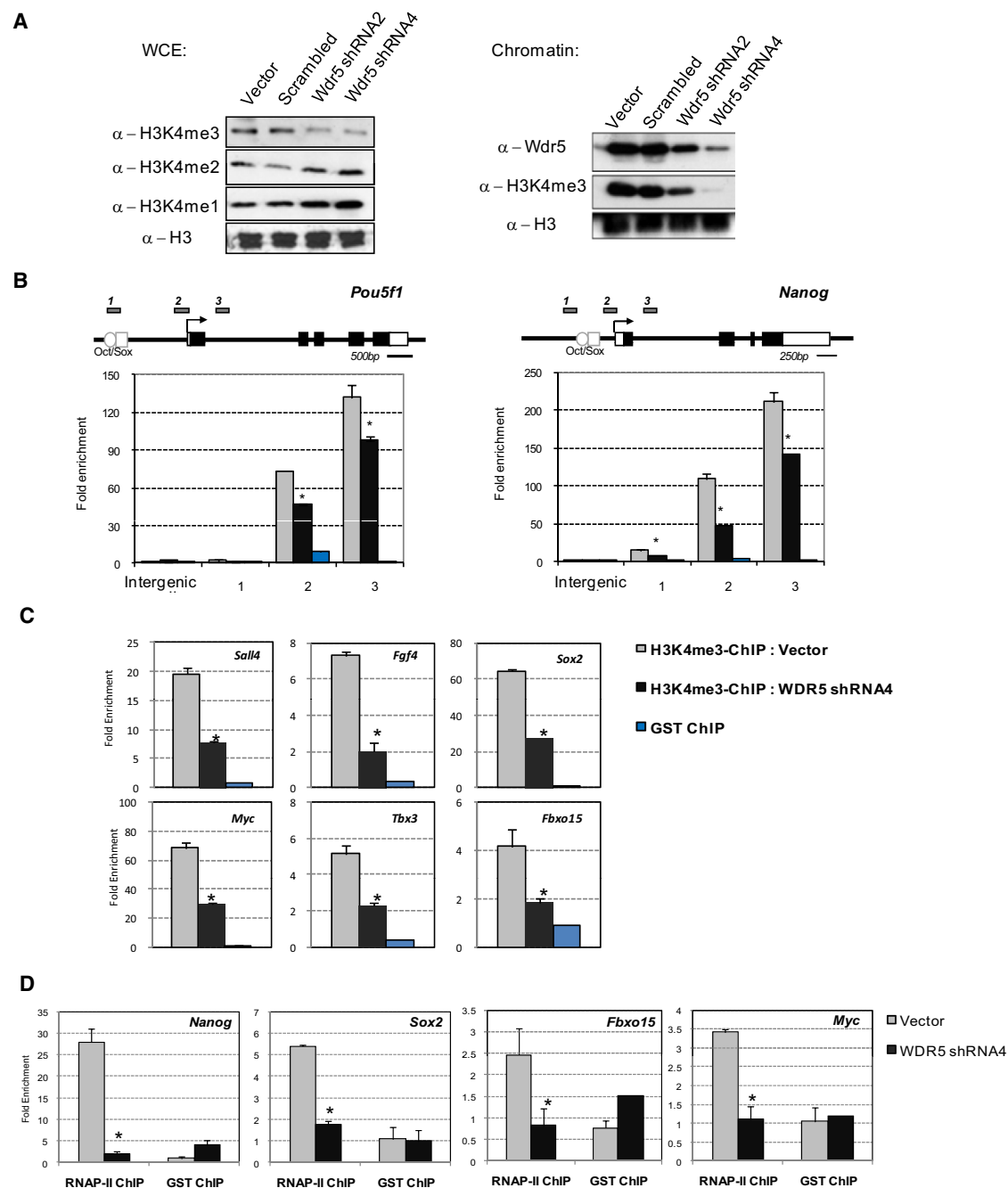


Figure 3. Wdr5 Maintains Global and Localized H3K4 Trimethylation

(A) Immunoblot after 4 days Wdr5 knockdown. WCE, whole-cell extract.

(B and C) ChIP-qPCR analysis of H3K4me3 mark at various loci after Wdr5 knockdown. Numbered gray bars indicate primer locations.

(D) ChIP-qPCR analysis of RNAP-II localization at various loci after Wdr5 knockdown. Values are expressed as fold enrichment relative to input DNA and a control region.

All data are represented as mean \pm SD; n = 3; *p < 0.005. See also Figure S3.

We continued to validate the Wdr5-Oct4 interaction using epitope-tagged proteins expressed in 293T cells (Figure 4C). Oct4-IP successfully pulled down Wdr5, whereas the reciprocal IP was less efficient, presumably because Wdr5 gets competed

away by endogenous interacting partners. We also performed an in vitro binding assay using recombinant Wdr5 and Oct4 (Figure 4D). Encouragingly, we observed co-IP of recombinant Wdr5 using an antibody specific for Oct4. However, this

pull-down was significantly weaker than in co-IPs in ES or 293T cells, suggesting that whereas Wdr5 and Oct4 are direct interaction partners, the interaction might be further stabilized in a multi-meric complex.

It was shown previously that strong Myc-DNA binding is positively correlated with “euchromatic clusters” that bear high H3K4me3 levels (Guccione et al., 2006). Therefore, we hypothesized that Oct4 binding to DNA may also be dependent on certain epigenetic features and be mediated through Wdr5. To investigate this, we performed a sequential peptide-IP experiment (Figure 4E, box). As expected, biotinylated-peptide pull-down assays demonstrated strong Wdr5 specificity toward the H3K4me3 peptide in stringent salt conditions (Figure S4G). Flag-IP of the Wdr5-Oct4 complex (IP1) followed by peptide-IP (IP2) demonstrated specificity of Oct4 for the H3K4me3 peptide. Increased salt concentration retained the affinity of Wdr5 for H3K4me3 but abolished the interaction with Oct4 (Figure 4E). These data point to indirect interactions of Oct4 with H3K4me3-modified histones, mediated by Wdr5, and suggest that portions of the ES cell genome that are “visible” to Oct4 could be restricted by higher-order chromatin organization.

Wdr5 and Oct4 Share Overlapping Gene Regulatory Functions

What is the functional importance of the Wdr5-Oct4 interaction? We postulated that Oct4 would be required to recruit Wdr5 to self-renewal-associated gene promoters, and this in turn maintains robust H3K4me3. Indeed, Oct4 depletion decreased Wdr5 binding as well as H3K4me3 modification at promoters (*Pou5f1*, *Nanog*, and *Sox2*) cobound by Wdr5 and Oct4 (Figure 4F). In contrast, at genes (*Adfp* and *Gnl3*) bound by Wdr5, but not by Oct4, we detected increased Wdr5 binding and H3K4me3 modification upon Oct4 depletion. This suggests that the Wdr5-Oct4 partnership performs specific roles at promoters of self-renewal genes and Wdr5 also performs discreet transcriptional functions without the participation of Oct4.

To assess the global extent of gene regulation, we compared differentially expressed genes upon depletion of Wdr5 or Oct4 (Table S2). 1532 and 646 genes were differentially expressed after Wdr5 or Oct4 knockdown, respectively, with 329 common genes (Figure 4G). Interestingly, GSEA showed high enrichment of Oct4-activated genes in control ES cells that become repressed upon Wdr5 depletion (Figure 4H and Figure S5A). Conversely, Oct4-repressed genes became enriched only upon loss of Wdr5. GSEA comparisons with published ChIP data sets of bivalent promoters and transcription factor binding targets provided additional evidence that Oct4 and Wdr5 share significant overlapping gene regulatory functions (Figure S5B and S5C).

Genome-wide Mapping of Wdr5, Rbbp5, H3K4me3, and Oct4 Localizations Using ChIP Sequencing

To determine the direct transcriptional targets of Oct4 and Wdr5, we mapped the DNA-binding sites for Wdr5 and Oct4, along with Rbbp5 and H3K4me3, by ChIP sequencing (Figure S6A). Comparison with published H3K4me3- and Oct4-ChIP-seq data sets exhibited strong overlap in target genes and local

binding profiles (data not shown), as well as high colocalization frequencies of binding regions (Figure 5D). Importantly, ChIP-qPCR validation revealed a low false discovery rate (FDR) for the identified binding regions (Figure S6B).

In support of our earlier observations (Figures 4G and 4H), the distributions of Oct4 and Wdr5 localization were strikingly similar (Figures 5A and 5B), wherein 75% of Oct4 target genes were co-bound by Wdr5 (Figure 5C). In line with a recent report (Kim et al., 2010), clustering of the colocalization frequencies of histone modifications, transcription factors, and transcriptional regulatory proteins recapitulated Polycomb (Figure 5D, blue), ES core (red), and Myc modules (green). Evidently, Oct4 and the core module share no significant overlap with regions of the genome marked by H3K27me3, H3K36me3, or H3K9me3 modifications. As expected, Wdr5 and Oct4 share a strong correlation in their binding regions and serve to bridge the Myc and the core modules (red-green). Lastly, the top Oct4-bound genes have significantly higher Wdr5 ChIP-seq signals than the bottom Oct4-bound genes (Figure 5E). The converse was also true, providing additional evidence that Oct4 and Wdr5 are partners in transcriptional regulation.

Wdr5, Rbbp5, and H3K4me3 binding regions are largely located within Refseq promoters (Figure 5A) and overrepresented in gene-rich chromosomal regions (Figure S6C) and share a strong overlap in their binding targets (Figure 6A). We identified 9303 Wdr5, Rbbp5, and H3K4me3 coassociated target genes, termed *trxG* hereafter. In line with the gene activation role of *trxG* (Ringrose and Paro, 2004), the level of mRNA expression in ES cells was directly proportional to the intensity of *trxG* ChIP-seq signals (Figure 6B). Lastly, a large proportion of *trxG* target genes contained “bivalent” domains (Table S3 and Figure S6D) and GO enrichment in categories like developmental processes, neurogenesis, embryogenesis, mesoderm, and ectoderm development (Figure S6E).

Oct4, Sox2, Nanog, and *trxG* Cooperate in Transcriptional Activation

We sought to understand the extent to which the known transcriptional network cooperates with *trxG* in gene regulation by broadening our analyses to include genes bound by *trxG* as well as Oct4 (this study), Sox2, and Nanog (Marson et al., 2008) (OSN) (Table S1). Oct4, Sox2, and Nanog are known to possess both transcriptional activation and repression functions, but the specific mechanisms that distinguish between these two properties remain elusive (Marson et al., 2008). We hypothesized that, because *trxG* is required for transcriptional activation (Ringrose and Paro, 2004), it would work with OSN specifically for this function. We identified four markers of active transcription from published reports (Marson et al., 2008; Mikkelsen et al., 2007; Rahl et al., 2010)—H3K79me2, H3K36me3, elongating RNAPII (–RNAPII–Ser2P), and Paf1 complex (Ctr9) binding—and a marker of repression, H3K27me3 (Mikkelsen et al., 2007). As described previously (Rahl et al., 2010), cMyc targets are highly positive for all four activation marks, whereas Suz12 targets are largely H3K27me3 positive (Figure 6C, top). Next, we observed *trxG* and Oct4 targets to be significantly activated above baseline levels. Additionally, target genes with OSN co-occupancy were preferentially more active than targets occupied by Oct4 alone,

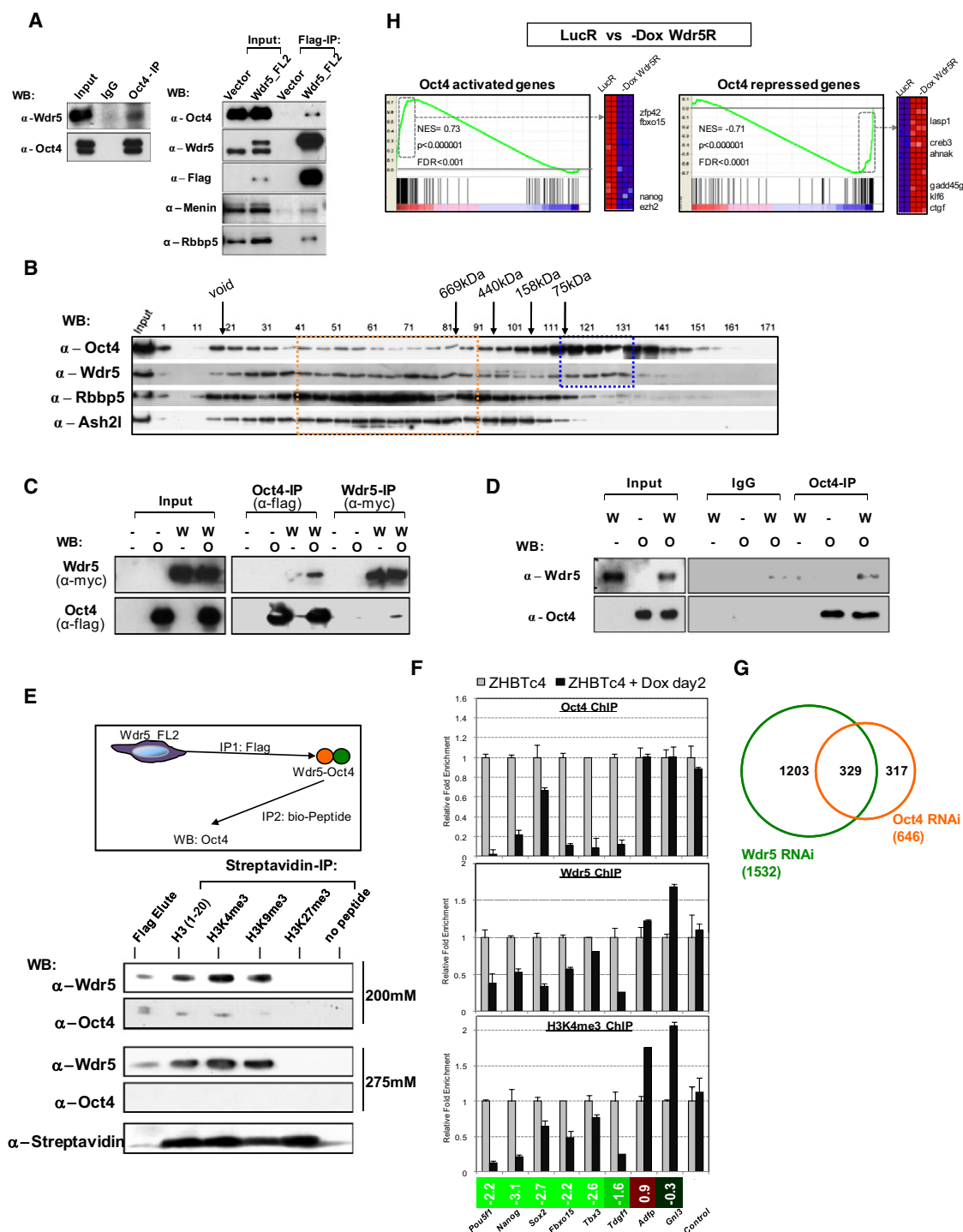


Figure 4. Oct4 Interacts with Wdr5 and Shares Overlapping Gene Regulatory Functions

(A) Co-IP shows Oct4 interaction with Wdr5. Oct4 pull-down of Wdr5 protein (left). Flag was used to IP for Wdr5 in Wdr5_FL2 line (right). IP was repeated three times. (B) Gel filtration analysis of ES cell nuclear extracts. Migration of molecular markers is indicated above the panels, and immunoblot antibodies are shown on the left. (C) Epitope-tagged co-IP in 293T cells. Flag-Oct4 (O) pulled down Myc-Wdr5 (W) and vice versa. Flag/myc antibodies were used for both IP and WB. Input shows equal expression. (D) In vitro binding assay using recombinant Oct4 (O) and Wdr5 (W). Proteins were immunoblotted after IP with Oct4 antibody. (E) Sequential peptide IP assay. Flag-mediated IP of Wdr5-Oct4 complex (IP1) and then biotin-peptide-mediated IP (IP2) shows Oct4 affinity for H3K4me3 peptide. IP2 was performed in 200 mM or 275 mM salt. Lane 1 (Flag elute) is protein extract before IP2. H3(1–20) represents the first 20 amino acids on unmodified H3. Streptavidin blot shows equal peptides IP'ed. (F) ChIP analysis of Oct4, Wdr5, and H3K4me3. Relative Fold Enrichment for Oct4 ChIP, Wdr5 ChIP, and H3K4me3 ChIP. Legend: ZHBTc4 (white), ZHBTc4 + Dox day2 (black). (G) Venn diagram showing overlapping genes between Wdr5 RNAi (1532) and Oct4 RNAi (646). Overlap: 329 genes.

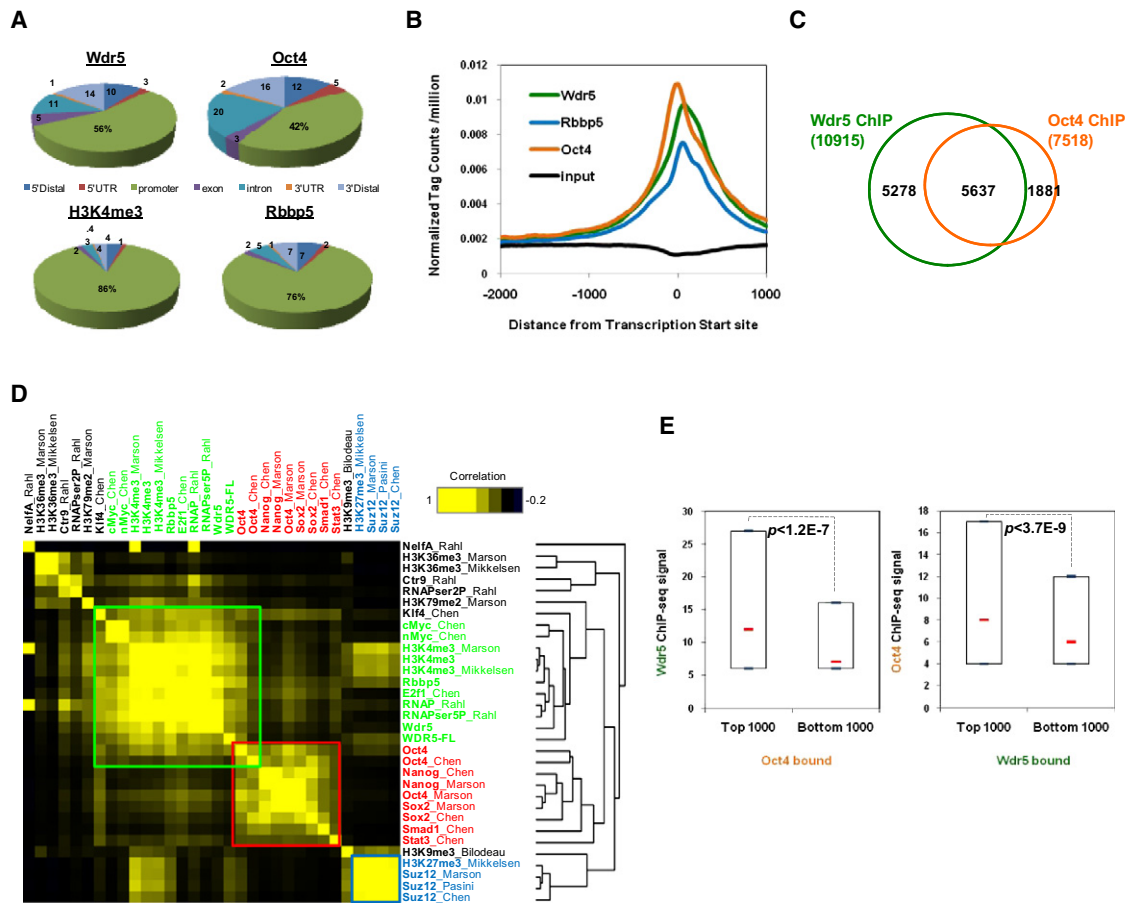


Figure 5. Genome-wide Mapping of Wdr5, Oct4, H3K4me3, and Rbbp5 Localizations Using ChIP-seq

(A) Percentage distribution of ChIP-seq binding regions relative to nearest Refseq genes for Wdr5, Rbbp5, H3K4me3, and Oct4.

(B) Distributions of Rbbp5, Wdr5, and Oct4 sequence tags relative to the transcription start site of 26412 RefSeq genes. Tag counts were normalized to total number of tags in each sequencing reaction.

(C) Venn diagram showing overlap of Wdr5- (green) and Oct4-bound (orange) genes.

(D) Heatmap of colocalization frequency of Wdr5, Rbbp5, H3K4me3, and Oct4 binding regions with published data sets (Bilodeau et al., 2009; Chen et al., 2008; Marson et al., 2008; Mikkelsen et al., 2007; Pasini et al., 2010; Rahl et al., 2010). Factors were hierarchically clustered using average linkage metric along both axes.

(E) Box plots show median (red bar), 25th, and 75th percentile number of ChIP-seq tags. Blue bars show 2.5th and 97.5th percentile.

See also Figure S6 and Table S4.

in line with the hypothesis that these transcription factors act synergistically for gene activation (Kim et al., 2008).

Five sectors, [I]–[V], of genes were identified based on their occupancies by *trxG* and/or OSN (Figure 6D) (Table S3). We then asked what is the percentage of genes in sectors [I]–[V] containing these marks of activation. Remarkably, the percentage of active genes was highest in sector [I] and was as high as that for cMyc, a strong transcriptional activator (Figure 6C, bottom). In contrast, the percentage of active genes was markedly reduced

in the absence of OSN or *trxG* co-occupancies, represented by sectors [II] and [III], respectively. This trend was not observed using the H3K27me3 repressive mark.

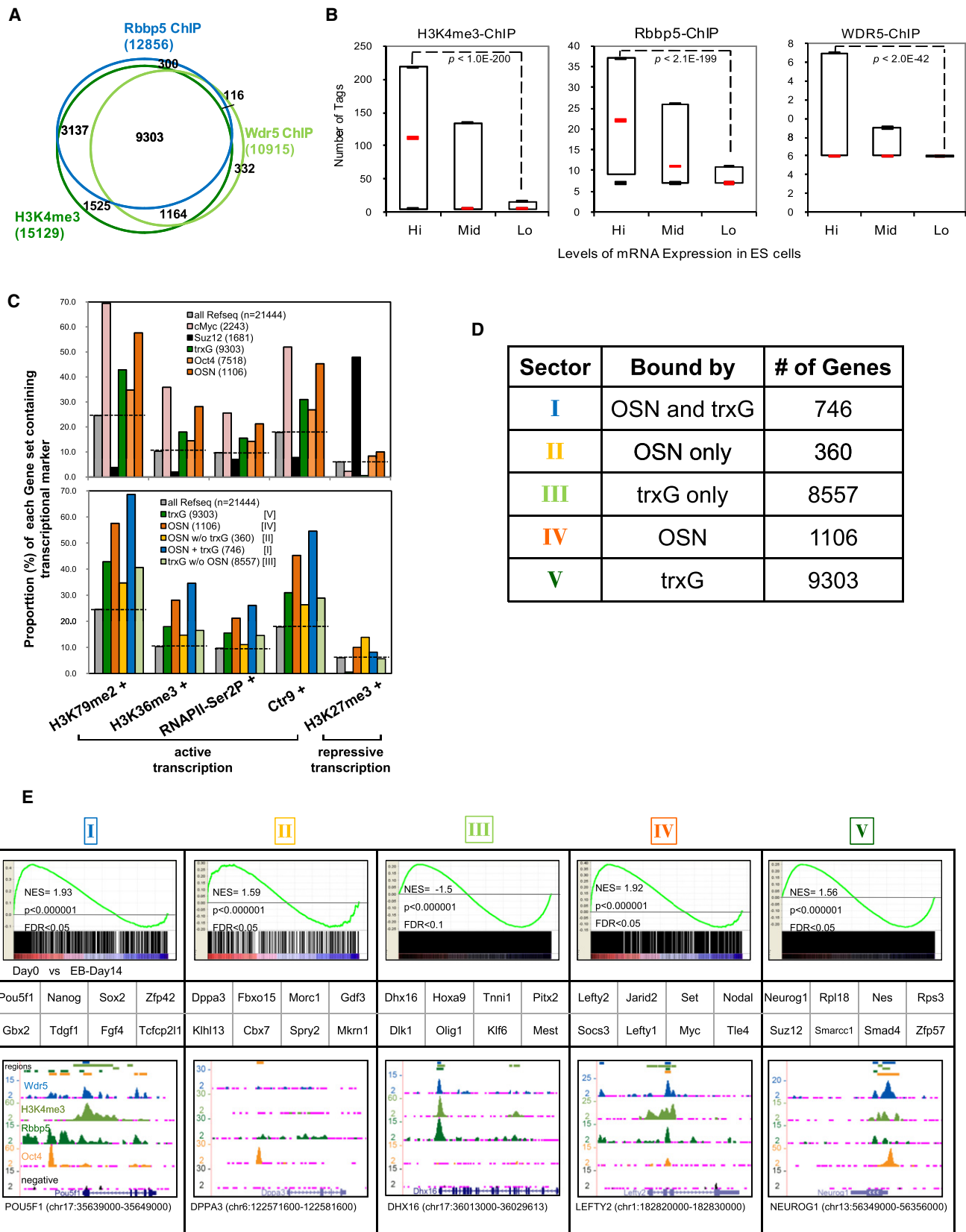
What are the properties of the genes in sectors [I], [II], and [III], and how do their expressions change upon differentiation? Using GSEA, we observed that: (1) OSN and *trxG* cobound genes (sector [I]) represented key self-renewal regulators (e.g., *Oct4*, *Nanog*, and *Sox2*) that are highly expressed in undifferentiated ES cells as indicated by a highly positive normalized

(F) ChIP-qPCR analysis of Oct4 binding and Wdr5 binding and H3K4me3 levels after 2 days Oct4 depletion. Values are expressed as fold enrichment relative to ZHBTc4. Control denotes intergenic region bound neither by Wdr5 nor Oct4. Heatmap shows Log₂ expression of genes upon Oct4 depletion. All data are represented as mean \pm SD; n = 3.

(G) Venn diagram of differentially expressed genes in Wdr5- and Oct4-depleted ES cells. p value for overlap as computed using Monte Carlo simulation is $< 1 \times 10^{-8}$.

(H) GSEA analyses of two gene sets representing Oct4-activated (left) and Oct4-repressed (right) genes. Heatmap represents top enriched genes. (Red, high expression; blue, low expression). Note the similarity to Figure S5A.

See also Figure S4, and Figure S5, and Table S2.



enrichment score (NES) of +1.93 (Figure 6E, column 1); (2) OSN without *trxG* cobound genes (sector [II]) represented “auxiliary” pluripotency-associated regulators (e.g., *Dppa3*, *Fbxo15*, and *Gdf3*). This gene set is not as highly expressed in ES cells, as indicated by a lowered NES of +1.59, and might share redundant functions with sector [I] genes (Figure 6E, column 2); (3) *trxG* without OSN cobound genes (sector [III]) represented primarily developmental regulators (e.g., *Dhx16*, *Hoxa9*, and *Tnni1*) that are highly expressed only in differentiated cells, as indicated by a highly negative NES of −1.5 (Figure 6E, column 3). These findings suggest that the OSN transcriptional circuitry and *trxG* are accomplices in transcriptional activation of key self-renewal genes.

Wdr5 Is Required for Efficient Somatic Cell Reprogramming

It remains unclear how OSKM with no immediate histone modification activities reconfigure the epigenome during somatic cell reprogramming. Notably, we observed upregulation of *Wdr5* during iPS cell generation (Figures 7A and 7B), which led us to hypothesize that Oct4 partners with *Wdr5* to reset the epigenome during iPS cell formation. Therefore, we asked whether *Wdr5* is indeed required for reprogramming of mouse embryonic fibroblast (MEF) from Oct4 GFP reporter mice (Figure S7A). Specific downregulation of *Wdr5* in MEFs (Figure S7B) reduced the number of iPS colonies, as scored by colony morphology (Figure S7C), Oct4 GFP expression (Figure 7C), and number of AP-positive colonies (Figure 7D). This observation was not due to an adverse effect of *Wdr5* depletion on the proliferative capacity of MEFs (Figure 7E and Figure S7D). Our cell-cycle analyses in 3T3 fibroblasts further support this observation (Figure 2I). Oct4-GFP-positive colonies emerging in the *Wdr5* knockdown cultures either had not been infected by the shRNA lentivirus or had silenced it, as determined by *Wdr5* RT-PCR (Figure S7E). We next asked whether *Wdr5* is required for the early/initiation phase or the later/expansion phase of reprogramming by depleting *Wdr5* before (day 5), simultaneously with (day 0), and after (day +4, +8) OSKM introduction. The most marked attenuation in iPS colony formation was observed when *Wdr5* was depleted during the initial stages of reprogramming (Figure 7F). Moreover, this reduction in iPS efficiency was measurable very early (day 8) in reprogramming using AP and SSEA1 as “surrogate” markers of pluripotency before endogenous Oct4 is activated (Figure 7G). This reduction was observed as late as day 20, arguing against a mere delay in reprogramming. Taken together, these data suggest that OSKM requires robust *Wdr5* activity for effective somatic cell reprogramming.

DISCUSSION

The significance of our study is three fold. First, our work represents the detailed characterization of a core *trxG* member in the maintenance of ES cell self-renewal. *PcG*-associated members have been well characterized in this context. Knockout ES cells for *PcG* have been established, genome-wide binding targets have been investigated in both mouse and human ES cells (Surface et al., 2010), and recently, multiple groups have performed *PcG* pull-down experiments to identify Jumonji domain proteins as critical mediators of pluripotency (Landeira and Fisher, 2010). In contrast, there exist few complementary studies for *trxG*-associated members. Although not a cell-/tissue-specific factor like Oct4, we observed that elevated *Wdr5* expression appears to be a unique and defining property of pluripotent ES and iPS cells. Despite the identification of bivalent domains, it is unclear whether the H3K4me3 modification is required for transcriptional activation of self-renewal genes. Here, we reduced H3K4me3 levels through the perturbation of a core *trxG* protein and observed significant attenuation in self-renewal gene expressions that eventually leads to the induction of differentiation. Reduction, but not complete ablation, of H3K4me3 in our shRNA experiments allowed us to observe this self-renewal defect. We predict that a complete removal of *Wdr5* and, consequently, the H3K4me3 mark would result in a possibly lethal phenotype that bypasses self-renewal maintenance. We have provided significant data to suggest that the consequence of losing *Wdr5* is, in part, mediated through the loss of H3K4me3. However, it remains possible that *Wdr5* interacts with other factors, apart from Oct4, and performs functions that are distinct from H3K4me3 modification that also could result in loss of pluripotency.

Additionally, our data supplements published work on Chd1 and Tip60-p400 complex. Chd1 was shown to be essential for open chromatin, pluripotency, and reprogramming (Gaspar-Maia et al., 2009). These results support our findings, as Chd1 is a “reader” of the H3K4me3 mark and our complementary results show *Wdr5* to be a “presenter” of H3K4. We indeed observed increased expression of H3K4me3 and acetylated H3K9/14 in ES cells compared to somatic cells, which presumably maintains the ES cell epigenome in its open and transcriptionally permissive state. Fazzio et al. reported that reduced H3K4me3 diminished Tip60-p400 recruitment to chromatin and induced loss of ES cell identity (Fazzio et al., 2008). These studies, including our work, collectively indicate that the H3K4me3 mark is an indispensable histone mark that regulates the balance between self-renewal and lineage commitment.

Figure 6. Oct4, Sox2, Nanog, and *trxG* Are Partners in Transcriptional Activation

(A) Venn diagram showing overlap of *Wdr5*, *Rbbp5*, and H3K4me3 ChIP target genes.
(B) 18096 Refseq genes were divided equally into three expression groups and were plotted against each ChIP-seq tag signal. Box plots show median (red bar), 25th, and 75th percentile number of ChIP-seq tags. Whiskers show 2.5th and 97.5th percentile.
(C) Proportion (%) of each gene set (colored bars), extracted from published (Chen et al., 2008; Marson et al., 2008) and current ChIP-seq data sets, containing markers of active and repressive transcription. *Wdr5*, *Rbbp5*, and H3K4me3 cobound (*trxG*). All Refseq (gray bar, black-dotted line) genes represent baseline %.
(D) Chart showing number of *trxG*- and OSN-bound genes subclassified into five sectors. [I], OSN and *trxG*; [II], OSN without *trxG*; [III], *trxG* without OSN; [IV], OSN_all; and [V], *trxG*_all.
(E) Table containing GSEA (top row) of mRNA expressions upon EB differentiation (Perez-Iratxeta et al., 2005), representative gene names (middle-row), and ChIP-seq binding profiles (bottom row) for genes in sectors [I]–[V]. See also Figure S6 and Table S1 and Table S3.

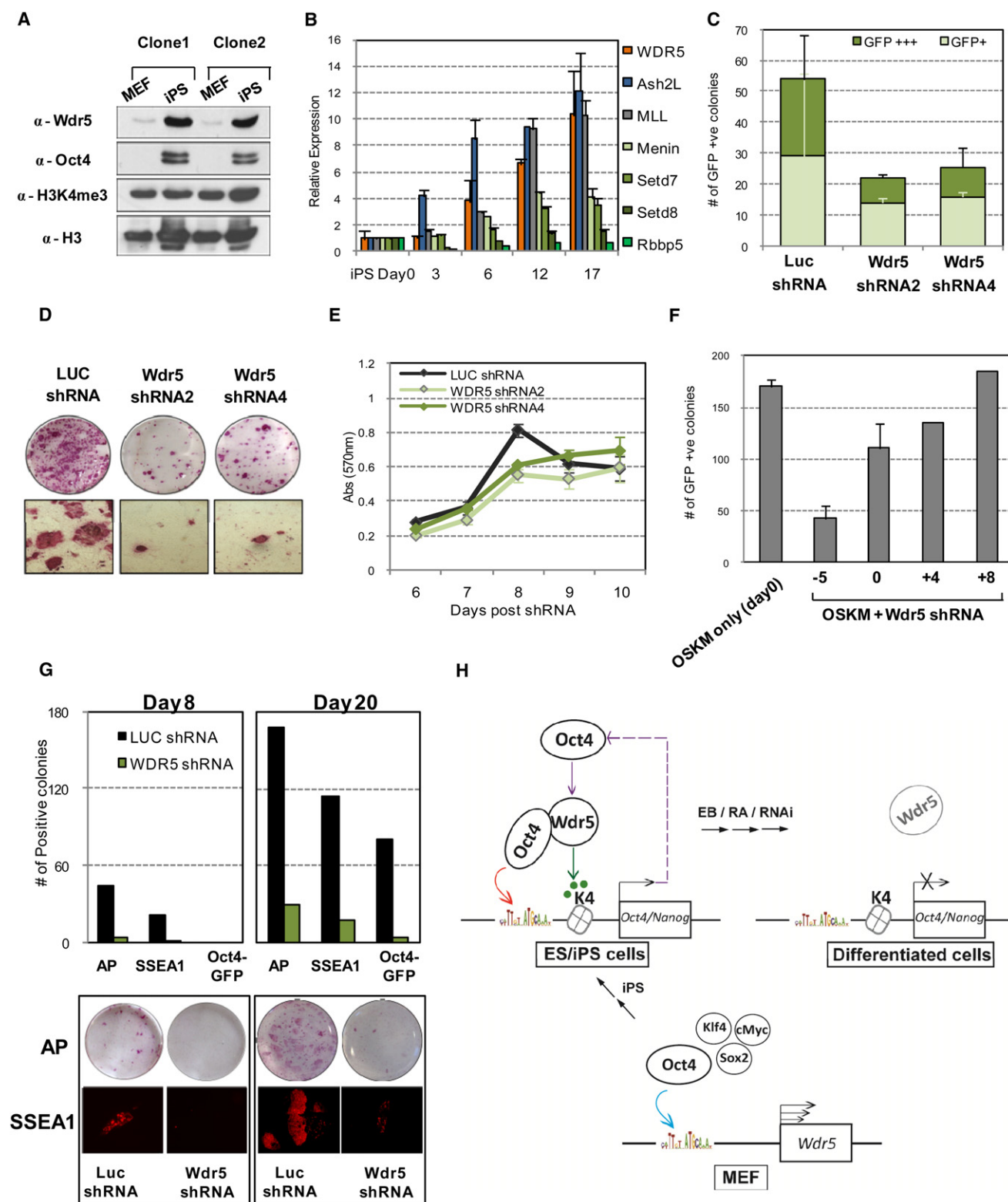


Figure 7. Increased Wdr5 Expression Is Required for Reprogramming of Oct4-GFP MEFs by Defined Factors

(A) Immunoblot of two independent iPS clones and their parental MEFs.

(B) Real-time PCR of *trxG*-associated members during iPS induction. Data are normalized to actin and are shown relative to MEF. Data are represented as mean \pm SD; n = 3.

Second, we put forward an integrated transcriptional network-epigenetic regulatory model for the maintenance of self-renewal. We and others have shown that H3K4me3 marks a large proportion of the ES cell genome, including promoters that are unrelated to self-renewal. How then can the self-renewal function of Wdr5/H3K4me3 be conferred? We propose that the locus specificity of Wdr5 is, in part, conferred through its direct and functional interaction with Oct4. We focused on the Oct4-Wdr5 interaction because Oct4 is a master regulator of pluripotency and is the only factor that until recently remained irreplaceable in reprogramming (Heng et al., 2010). However, at least in some experiments, we did observe co-IP of Sox2 and Nanog, suggesting that Wdr5 may interact with a more extensive complex of transcription factors. A recent study reported an Oct4-interactome of 166 proteins, which included transcription factors and chromatin-modifying complexes, many of which were not previously known to associate with the ES cell network (Dejosez et al., 2010; van den Berg et al., 2010). The Wdr5-Oct4 interaction was also observed there. Our mechanistic work on Wdr5 therefore elucidates the functional importance of this interaction and possibly sheds light on the relevance of Oct4's surprisingly broad range of interaction partners. We also determined that *trxG* and the OSN-triad colocalize at key self-renewal regulatory genes and synergistically maintain their robust expression levels. Gene promoters that are only OSN bound or only *trxG* bound are less likely to be transcriptionally active in ES cells. Our genome-wide localization analyses of Wdr5 and Rbbp5 represent the first unbiased, high-resolution mapping of core *trxG* member occupancy in any cell/tissue type and thus provide a valuable resource for future investigation of *trxG*-mediated gene regulation and potential TRE-motif discovery (Table S4).

Lastly, we established that Wdr5 is required for the initial reconfiguration phase of somatic cell reprogramming. We propose that the Wdr5-Oct4 partnership accomplishes this as follows (Figure 7H). First, Oct4 enhances basal Wdr5 expression in MEFs (blue arrow) through direct binding and transcriptional activation of its promoter. Next, the DNA specificity conferred by Oct4 directs Wdr5 to genomic loci encoding self-renewal genes, such as *Pou5f1* and *Nanog*, to re-establish a H3K4me3 high chromatin signature (green arrow). This elevated expression of H3K4me3 subsequently facilitates strong Oct4 occupancy to direct robust transcriptional activation (red arrow), presumably in conjunction with the larger *trxG* complex. Finally, the positive feedback loop set up by Oct4 targeting *Wdr5* (purple arrows) allows for the establishment of iPS cells or the maintenance of ES cell self-renewal. EB and RA differentiation or *trxG* member depletion compromises the maintenance of self-renewal and triggers differentiation.

In summary, the work presented here elucidates a previously unrecognized interconnectivity between the core transcriptional network and select members of the *trxG* complex, reveals important insights into the role of Wdr5/H3K4me3 in the maintenance of ES cell self-renewal, and suggests how Oct4 downstream target epigenetic factors reconfigure the H3K4me3 signature during the process of somatic cell reprogramming.

EXPERIMENTAL PROCEDURES

Cell Culture and Differentiation Assays

Mouse ES cell lines—E14T, CCE, J1, ZHBTc4, NanogR, and Wdr5R—were cultured and differentiated as previously described (Ivanova et al., 2006). Dermal papilla, dermal fibroblasts, and MEFs were derived as described previously (Tsai et al., 2010).

Gene Expression Microarray, GO, and GSEA

Microarrays were conducted on Illumina Beadchip arrays. All data were normalized using LumiR. Differentially expressed genes were identified using Limma: $\text{Log}_2\text{FC} > 0.6$ or < -0.6 ; adjusted p value < 0.05 ; and detection probability > 0.99 . Microarray data deposited at GEO (GSE19588). Cluster 3.0 and Java Treeview were used for data visualization. GO was performed at <http://www.pantherdb.org/>. GSEA was performed at <http://www.broadinstitute.org/gsea/>.

Real-Time Quantitative PCR and Immunoblotting

Total RNA was Trizol extracted, column purified, and reverse transcribed using the High Capacity kit (Applied Biosystems). For ChIP-qPCR analysis, 1 ng ChIP-DNA was used for each PCR. All qPCR analyses were performed using Fast SYBR Green (Applied Biosystems). To obtain whole-cell protein extracts, cells were lysed in RIPA buffer. Primer sequences and antibodies are available in Supplemental Information and Table S6.

Short Hairpin RNA Design

Target sequences: Wdr5 shRNA2, GCCGTTTCATTTCAACCGTGAT; Wdr5 shRNA4, GCAAGTTCATCTGCTGATA; Oct4 shRNA, GAAGGATGTGGTTTCGA GTA; Nanog shRNA, GAACTATTCTTGCTTACAA; Menin shRNA, GTAGATTT CCGCACTTTAT; and Ash2l shRNA, CGAGTCTGTGTTAGCCCTACAT.

Co-IP and ChIP Assay

ES cells were lysed in Buffer G, incubated overnight with 5 μg antibody, and captured with Protein G beads. Protein complexes were eluted by boiling in loading buffer. 10 μl was used for each immunoblot with 2% input. Epitope-tagged co-IP in 293T cells was performed with Flag and Myc antibodies in Buffer G. ChIP was performed as described previously (Schanuel et al., 2009).

Biotinylated Peptide IP

Biotinylated peptides were synthesized and conjugated to streptavidin beads. ES cell extracts were prepared in Buffer G and incubated with peptide-conjugated beads. Beads were washed and eluted in loading buffer.

Gel Filtration and In Vitro Binding Assay

Gel filtration was performed in DuoFlow BioLogic System according to manufacturer's manual (Biorad). In vitro binding assay was conducted in Buffer G with purified Pou5f1 and Wdr5 (Origene).

(C) High and low GFP-positive colonies were counted 14 days post-OSKM in Wdr5 and Luc knockdown cells. Data are represented as mean \pm SD.

(D) AP staining of entire wells (circles) and representative colonies (squares) from Wdr5 and Luc knockdown iPS colonies at day 14.

(E) MTT proliferation assay of MEF transduced with Luc or Wdr5 shRNA.

(F) Wdr5 depletion during iPS reprogramming. GFP⁺⁺⁺ colonies counted at day 14. OSKM only did not receive Wdr5 shRNA.

(G) AP, SSEA1, and GFP intensity assessed at early (day 8) or late stages (day 20) of iPS induction with (green bar) or without (black bar) Wdr5 shRNA. AP staining of entire wells (circles) and representative SSEA1 colonies (squares) is depicted.

(H) Proposed model.

See also Figure S7.

Generation of iPS Cells

As described previously (Tsai et al., 2010), Oct4-GFP MEFs were transduced with pMX-Oct4, Sox2, Klf4, and cMyc retroviruses and were cultured in ES media on irradiated MEFs. GFP-positive colonies were counted after 14 days posttransduction.

ChIP Sequencing and Data Analysis

ChIPed DNA was blunt ended, linker ligated, amplified, and applied to the flow-cell using the Solexa Cluster Station (Illumina). Samples were subjected to 36 cycles of sequencing using the Genome Analyzer II (Illumina) (see Table S5). Images acquired were processed through the image extraction pipeline and aligned to mouse NCBI build mm9 using ELAND. ChIP-seq data was deposited at GEO (GSE22934).

ACCESSION NUMBERS

All microarray data are deposited at GEO database with project number GSE19588. All ChIP-seq data are deposited at GEO database with project number GSE22934.

SUPPLEMENTAL INFORMATION

Supplemental Information includes Extended Experimental Procedures, seven figures, and six tables and can be found with this article online at doi:10.1016/j.cell.2011.03.003.

ACKNOWLEDGMENTS

We thank C.D. Allis, C. Hughes, J. Wysocka, A. Sevilla, X. Carvajal-Vergara, F. Pereira, A. Waghra, S. Pardo, S. Mendez-Ferrer, W.L. Tam, B. Lim, C. Ren, H.A. Wu, J. Gengold, and V. Nair for technical assistance, materials, and advice. This work was supported by NIH (R01GM078465) to I.R.L.; NYSTEM (C024410) to I.R.L. and C.S.; and NYSTEM (C024285) to E.B. D.F.L. is a NYSCF Fellow. M.R. is supported by a Dermatology Foundation Career Development Award.

Author contributions: Y.-S.A., conception and design, collection and analysis of data, manuscript writing, final approval of manuscript; S.-Y.T., D.-F.L., J.M., J.S., K.R., J.D., Y.G., and H.D., collection and analysis of data; J.W., B.C., M.R., manuscript writing; E.B., conception and design and manuscript writing; C.S., conception and design, data collection, and manuscript writing; I.R.L., conception and design, financial support, manuscript writing, and final approval of manuscript.

Received: September 23, 2010

Revised: December 22, 2010

Accepted: February 9, 2011

Published online: April 7, 2011

REFERENCES

- Bernstein, B.E., Mikkelsen, T.S., Xie, X., Kamal, M., Huebert, D.J., Cuff, J., Fry, B., Meissner, A., Wernig, M., Plath, K., et al. (2006). A bivalent chromatin structure marks key developmental genes in embryonic stem cells. *Cell* 125, 315–326.
- Bilodeau, S., Kagey, M.H., Frampton, G.M., Rahl, P.B., and Young, R.A. (2009). SetDB1 contributes to repression of genes encoding developmental regulators and maintenance of ES cell state. *Genes Dev.* 23, 2484–2489.
- Boyer, L.A., Plath, K., Zeitlinger, J., Brambrink, T., Medeiros, L.A., Lee, T.I., Levine, S.S., Wernig, M., Tajonar, A., Ray, M.K., et al. (2006). Polycomb complexes repress developmental regulators in murine embryonic stem cells. *Nature* 441, 349–353.
- Cao, F., Chen, Y., Cierpicki, T., Liu, Y., Basur, V., Lei, M., and Dou, Y. (2010). An Ash2L/RbBP5 heterodimer stimulates the MLL1 methyltransferase activity through coordinated substrate interactions with the MLL1 SET domain. *PLoS ONE* 5, e14102.

Carvajal-Vergara, X., Sevilla, A., D'Souza, S.L., Ang, Y.S., Schaniel, C., Lee, D.F., Yang, L., Kaplan, A.D., Adler, E.D., Rozov, R., et al. (2010). Patient-specific induced pluripotent stem-cell-derived models of LEOPARD syndrome. *Nature* 465, 808–812.

Chen, X., Xu, H., Yuan, P., Fang, F., Huss, M., Vega, V.B., Wong, E., Orlov, Y.L., Zhang, W., Jiang, J., et al. (2008). Integration of external signaling pathways with the core transcriptional network in embryonic stem cells. *Cell* 133, 1106–1117.

Couture, J.F., Collazo, E., and Trievel, R.C. (2006). Molecular recognition of histone H3 by the WD40 protein WDR5. *Nat. Struct. Mol. Biol.* 13, 698–703.

Dejosez, M., Levine, S.S., Frampton, G.M., Whyte, W.A., Stratton, S.A., Barton, M.C., Gunaratne, P.H., Young, R.A., and Zwaka, T.P. (2010). Ronin/Hcf-1 binds to a hyperconserved enhancer element and regulates genes involved in the growth of embryonic stem cells. *Genes Dev.* 24, 1479–1484.

Dou, Y., Milne, T.A., Ruthenburg, A.J., Lee, S., Lee, J.W., Verdine, G.L., Allis, C.D., and Roeder, R.G. (2006). Regulation of MLL1 H3K4 methyltransferase activity by its core components. *Nat. Struct. Mol. Biol.* 13, 713–719.

Efroni, S., Duttagupta, R., Cheng, J., Dehghani, H., Hoepfner, D.J., Dash, C., Bazett-Jones, D.P., Le Grice, S., McKay, R.D., Buetow, K.H., et al. (2008). Global transcription in pluripotent embryonic stem cells. *Cell Stem Cell* 2, 437–447.

Fazio, T.G., Huff, J.T., and Panning, B. (2008). An RNAi screen of chromatin proteins identifies Tip60-p400 as a regulator of embryonic stem cell identity. *Cell* 134, 162–174.

Gaspar-Maia, A., Alajem, A., Polesso, F., Sridharan, R., Mason, M.J., Heidrich, A., Ramalho-Santos, J., McManus, M.T., Plath, K., Meshorer, E., and Ramalho-Santos, M. (2009). Chd1 regulates open chromatin and pluripotency of embryonic stem cells. *Nature* 460, 863–868.

Guccione, E., Martinato, F., Finocchiaro, G., Luzzi, L., Tizzoni, L., Dall'Olio, V., Zardo, G., Nervi, C., Bernard, L., and Amati, B. (2006). Myc-binding-site recognition in the human genome is determined by chromatin context. *Nat. Cell Biol.* 8, 764–770.

Heng, J.C., Feng, B., Han, J., Jiang, J., Kraus, P., Ng, J.H., Orlov, Y.L., Huss, M., Yang, L., Lufkin, T., et al. (2010). The nuclear receptor Nr5a2 can replace Oct4 in the reprogramming of murine somatic cells to pluripotent cells. *Cell Stem Cell* 6, 167–174.

Ivanova, N., Dobrin, R., Lu, R., Kotenko, I., Levorse, J., DeCoste, C., Schafer, X., Lun, Y., and Lemischka, I.R. (2006). Dissecting self-renewal in stem cells with RNA interference. *Nature* 442, 533–538.

Karnik, S.K., Chen, H., McLean, G.W., Heit, J.J., Gu, X., Zhang, A.Y., Fontaine, M., Yen, M.H., and Kim, S.K. (2007). Menin controls growth of pancreatic beta-cells in pregnant mice and promotes gestational diabetes mellitus. *Science* 318, 806–809.

Kim, J., Chu, J., Shen, X., Wang, J., and Orkin, S.H. (2008). An extended transcriptional network for pluripotency of embryonic stem cells. *Cell* 132, 1049–1061.

Kim, J., Woo, A.J., Chu, J., Snow, J.W., Fujiwara, Y., Kim, C.G., Cantor, A.B., and Orkin, S.H. (2010). A Myc network accounts for similarities between embryonic stem and cancer cell transcription programs. *Cell* 143, 313–324.

Lairmore, T.C., and Chen, H. (2009). Role of menin in neuroendocrine tumorigenesis. *Adv. Exp. Med. Biol.* 668, 87–95.

Landeira, D., and Fisher, A.G. (2010). Inactive yet indispensable: The tale of Jarid2. *Trends Cell Biol.* 21, 74–80.

Loh, Y.H., Zhang, W., Chen, X., George, J., and Ng, H.H. (2007). Jmjd1a and Jmjd2c histone H3 Lys 9 demethylases regulate self-renewal in embryonic stem cells. *Genes Dev.* 21, 2545–2557.

Marson, A., Levine, S.S., Cole, M.F., Frampton, G.M., Brambrink, T., Johnstone, S., Guenther, M.G., Johnston, W.K., Wernig, M., Newman, J., et al. (2008). Connecting microRNA genes to the core transcriptional regulatory circuitry of embryonic stem cells. *Cell* 134, 521–533.

Mikkelsen, T.S., Ku, M., Jaffe, D.B., Issac, B., Lieberman, E., Giannoukos, G., Alvarez, P., Brockman, W., Kim, T.K., Koche, R.P., et al. (2007). Genome-wide

maps of chromatin state in pluripotent and lineage-committed cells. *Nature* 448, 553–560.

Pasini, D., Bracken, A.P., Hansen, J.B., Capillo, M., and Helin, K. (2007). The polycomb group protein Suz12 is required for embryonic stem cell differentiation. *Mol. Cell. Biol.* 27, 3769–3779.

Pasini, D., Cloos, P.A., Walfridsson, J., Olsson, L., Bukowski, J.P., Johansen, J.V., Bak, M., Tommerup, N., Rappsilber, J., and Helin, K. (2010). JARID2 regulates binding of the Polycomb repressive complex 2 to target genes in ES cells. *Nature* 464, 306–310.

Perez-Iratxeta, C., Palidwor, G., Porter, C.J., Sanche, N.A., Huska, M.R., Suomela, B.P., Muro, E.M., Krzyzanowski, P.M., Hughes, E., Campbell, P.A., et al. (2005). Study of stem cell function using microarray experiments. *FEBS Lett.* 579, 1795–1801.

Pullirsch, D., Härtel, R., Kishimoto, H., Leeb, M., Steiner, G., and Wutz, A. (2010). The Trithorax group protein Ash2l and Saf-A are recruited to the inactive X chromosome at the onset of stable X inactivation. *Development* 137, 935–943.

Rahl, P.B., Lin, C.Y., Seila, A.C., Flynn, R.A., McQuine, S., Burge, C.B., Sharp, P.A., and Young, R.A. (2010). c-Myc regulates transcriptional pause release. *Cell* 141, 432–445.

Ringrose, L., and Paro, R. (2004). Epigenetic regulation of cellular memory by the Polycomb and Trithorax group proteins. *Annu. Rev. Genet.* 38, 413–443.

Schaniel, C., Ang, Y.S., Ratnakumar, K., Cormier, C., James, T., Bernstein, E., Lemischka, I.R., and Paddison, P.J. (2009). Smarcc1/Baf155 couples self-renewal gene repression with changes in chromatin structure in mouse embryonic stem cells. *Stem Cells* 27, 2979–2991.

Schuettengruber, B., Chourrout, D., Vervoort, M., Leblanc, B., and Cavalli, G. (2007). Genome regulation by polycomb and trithorax proteins. *Cell* 128, 735–745.

Shilatifard, A. (2006). Chromatin modifications by methylation and ubiquitination: implications in the regulation of gene expression. *Annu. Rev. Biochem.* 75, 243–269.

Stoller, J.Z., Huang, L., Tan, C.C., Huang, F., Zhou, D.D., Yang, J., Gelb, B.D., and Epstein, J.A. (2010). Ash2l interacts with Tbx1 and is required during early embryogenesis. *Exp. Biol. Med. (Maywood)* 235, 569–576.

Surface, L.E., Thornton, S.R., and Boyer, L.A. (2010). Polycomb group proteins set the stage for early lineage commitment. *Cell Stem Cell* 7, 288–298.

Tam, W.L., Lim, C.Y., Han, J., Zhang, J., Ang, Y.S., Ng, H.H., Yang, H., and Lim, B. (2008). T-cell factor 3 regulates embryonic stem cell pluripotency and self-renewal by the transcriptional control of multiple lineage pathways. *Stem Cells* 26, 2019–2031.

Tay, Y.M., Tam, W.L., Ang, Y.S., Gaughwin, P.M., Yang, H., Wang, W., Liu, R., George, J., Ng, H.H., Perera, R.J., et al. (2008). MicroRNA-134 modulates the differentiation of mouse embryonic stem cells, where it causes post-transcriptional attenuation of Nanog and LRH1. *Stem Cells* 26, 17–29.

Taylor, M.D., Sadhukhan, S., Kottangada, P., Ramgopal, A., Sarkar, K., D'Silva, S., Selvakumar, A., Candotti, F., and Vyas, Y.M. (2010). Nuclear role of WASp in the pathogenesis of dysregulated TH1 immunity in human Wiskott-Aldrich syndrome. *Sci. Transl. Med.* 2, 37ra44.

Thomson, J.P., Skene, P.J., Selfridge, J., Clouaire, T., Guy, J., Webb, S., Kerr, A.R., Deaton, A., Andrews, R., James, K.D., et al. (2010). CpG islands influence chromatin structure via the CpG-binding protein Cfp1. *Nature* 464, 1082–1086.

Tsai, S.Y., Clavel, C., Kim, S., Ang, Y.S., Grisanti, L., Lee, D.F., Kelley, K., and Rendl, M. (2010). Oct4 and klf4 reprogram dermal papilla cells into induced pluripotent stem cells. *Stem Cells* 28, 221–228.

Tyagi, S., and Herr, W. (2009). E2F1 mediates DNA damage and apoptosis through HCF-1 and the MLL family of histone methyltransferases. *EMBO J.* 28, 3185–3195.

van den Berg, D.L., Snoek, T., Mullin, N.P., Yates, A., Bezstarosti, K., Demmers, J., Chambers, I., and Poot, R.A. (2010). An Oct4-centered protein interaction network in embryonic stem cells. *Cell Stem Cell* 6, 369–381.

Wang, P., Lin, C., Smith, E.R., Guo, H., Sanderson, B.W., Wu, M., Gogol, M., Alexander, T., Seidel, C., Wiedemann, L.M., et al. (2009). Global analysis of H3K4 methylation defines MLL family member targets and points to a role for MLL1-mediated H3K4 methylation in the regulation of transcriptional initiation by RNA polymerase II. *Mol. Cell. Biol.* 29, 6074–6085.

Wysocka, J., Swigut, T., Milne, T.A., Dou, Y., Zhang, X., Burlingame, A.L., Roeder, R.G., Brivanlou, A.H., and Allis, C.D. (2005). WDR5 associates with histone H3 methylated at K4 and is essential for H3 K4 methylation and vertebrate development. *Cell* 121, 859–872.

Zhu, E.D., Demay, M.B., and Gori, F. (2008). Wdr5 is essential for osteoblast differentiation. *J. Biol. Chem.* 283, 7361–7367.